FACTA UNIVERSITATIS
Series: **Mechanics, Automatic Control and Robotics** Vol.3, N° 13, 2003, pp. 583 - 597

AN R-CURVE ASSESSMENT OF STABLE CRACK GROWTH IN AN ALUMINIUM ALLOY

UDC 539.219.2 620.1

A. R. Luxmoore

Faculty of Engineering, University of Wales Swansea, UK

Abstract. *An AlMgZn alloy has shown brittle behaviour when tested using standard fracture specimens, but larger specimens with the same contour geometry have produced stable fracture i.e. controlled crack propagation under either increasing load or increasing displacement. An R-curve analysis produced a rather unusually shaped, but unique, R-curve for the alloy, with the crack resistance increasing parabolically with crack extension. In addition, crack initiation was indexed by the constraint of the test specimen. Despite these complications, the R-curve analysis allowed a satisfactory explanation for the different fracture behaviour between the small and large test specimens. The parabolic nature of the R-curve, obtained from several different geometries, suggested that a simple shear lip analysis, similar to that of Krafft, Boyle and Sullivan, should explain the behaviour of the test pieces, but despite some modifications to the original shear lip theory, the results are not conclusive.*

Nomenclature

Abbreviations:

ASTM	American Society for Testing and Materials
CCT	Centre Cracked specimens in Tension
COD	Crack Opening Displacement (at any point along crack flank)
CMOD	Crack Mouth Opening Displacement
CT	Compact Tension specimen
SSY	Small Scale Yielding
2-D	Two-dimensional
3-D	Three-dimensional
3PB	Three Point Bend specimen

Received October 20, 2002

Latin symbols:

a	half-crack length (CCT specimen), crack length (3PB and CT specimens)
a_{eff}	a crack length assuming plasticity (in small scale yielding) at the crack tip
B	specimen thickness
b	ligament length
E	Young's modulus
G	the driving force
G_{eff}	the driving force for a effective crack length
J	the J-integral
J_C	J value at instability
J_e	elastic component of J
J_{IC}	fracture toughness in terms of J
J_p	plastic component of J
J_R	fracture resistance in terms of J
K	stress intensity factor
K_{IC}	plane strain fracture toughness
K_{eff}	stress intensity factor with respect to the effective crack length
R	fracture resistance
S	the ratio of total width of shear lips to specimen thickness.
W	specimen width
W_t	total energy dissipated during crack extension
W_e	energy dissipated due to crack extension alone
W_p	plastic energy dissipated in shear lips during crack growth

Greek symbols:

Δa or da	crack extension
Δa_{trans}	maximum crack extension for flat fracture zone

INTRODUCTION

A weldable AlMgZn alloy, similar in specification to 7019 alloy, has been developed for lightweight structural applications. Standard fracture tests produced valid plane strain K_{IC} values of around 35MPa√m. A full scale fatigue test on a structural component by Webber [1] showed an unexpected increase in fracture resistance compared with its plane strain $K_{IC.}$ An early study [2] attributed this increase to the loss of in-plane constraint in the structure.

The constraint effects were examined experimentally by Sumpter [3], using 3PB and CCT specimens of the bridge alloy. Henry *et al.* [4] combined experimental and finite element studies on the T and Q-stresses for these test specimens to show that the variation of critical J values, J_C, could be rationalised by an indexing parameter, i.e. using either the T-stress [5] or the Q-values [6]. These results led to the application of practical two-parameter failure criteria, in the form of J_C-T and J_C-Q loci. Henry and Luxmoore [2] showed that the structural component was a low constraint geometry, and introduced a fracture assessment scheme [7] using the J_C-T locus, Figure 1, and the applied J and T-stress for a given crack length. According to this scheme, a crack is unsafe when its combination of J and T-stress exceeds the locus.

Sumpter [3] noted that crack extension in a large (b >> B) fracture test specimen was stable, whilst shallow cracks in small (b = B) specimens failed at maximum loads. However, crack growth in all high constraint geometries, whether large or small, initiated at a constant J_{IC} value of 0.018MN/m (equivalent to $K_{IC} = 35MPa\sqrt{m}$). In all specimens, fracture surfaces consisted of a central flat fracture 'tunnel', with differing amounts of slant fracture near the specimen surfaces. The slant fracture was associated with the development of shear lips at the specimen surface. In the small specimens, the shear lips at the edge of the growing crack (as indicated by the slant fracture) reached a maximum width of 2-5 mm, but in the large specimens, they kept increasing until the fracture surface became fully slant, and the central flat fracture reached a point. Further crack growth was then fully slanted.

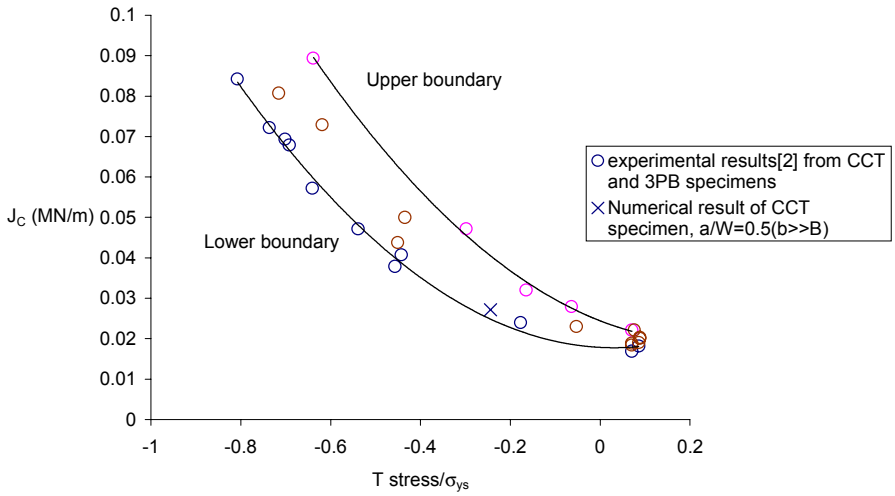

Fig. 1. J_C-T locus [2] and indexed value of J from a CCT specimen.

Resistance (R) curves were determined for stable crack extension in two large (b >> B) and a small (b = B) test specimens, and compared with R-curves from Sumpter. Fracture resistance is represented by the J-integral, denoted by J_R, where the subscript R denotes values of J on the resistance curve. The analyses produced concave J_R-curves, where the fracture resistance rises increasingly with crack extension, corresponding to the increasing width of the shear lips. This allows long cracks to be safe because, although $G > J_R$ at initiation, the rate of change $dG/da < dJ_R/da$ (the rate of change in fracture resistance) at, and after, this point. Using the R-curve approach, it is shown that further extension of long cracks is only possible by stable propagation under substantial load increases, agreeing with the experimental results of Sumpter [8]. A J_R-curve from a large CCT specimen (low constraint geometry) showed that the J_R values at initiation were elevated, but the curve coincided with that from high constraint geometries after further crack extension. Hence the fracture toughness (K_{IC}), and the values of J_R for low constraint geometries, must be indexed by T-stresses to allow for losses of constraint.

For the high constraint specimens, a concave parabola could fit the R-curves quite accurately, and a simple shear lip analysis was undertaken to explain the R-curve behaviour. This has not produced an entirely satisfactory model.

NUMERICAL ANALYSIS OF STABLE CRACK EXTENSION

Sumpter [3] conducted fracture toughness tests on the AlMgZn alloy using standard (b = B) 3PB specimens (for valid K_{IC} test), with a range of a/W from 0.05 to 0.5. A large 3PB and a large CCT specimen (for the same thickness but with b >> B) were also tested and these produced significant stable crack extension (see Table 1 for details). The effect of ligament size was shown by the alteration of the fracture plane, which changed from predominantly flat fracture in the square ligament (b = B) to slant fracture in the rectangular ligament (b >> B) for the same thickness. The shear lips developed and caused the initial flat fracture in the (b >> B) specimen to taper to a point (tunneling), whereas flat fracture was dominant throughout crack extension in the (b = B) specimens [3].

Table 1. Details of the finite element models for 3PB and CCT specimens.

3PB specimens a/W	Ligament length, b (mm)	Crack length, a (mm)	Span, S (mm)	Thickness, B (mm)
0.2 (b = B)	25	6.25	125	25
0.33	50	25	300	25
0.5	25	25	200	25
0.2(b >> B)	160	40	800	25
CCT specimen 2a/W				
0.52	62.5	67.5		25

Stable crack growth in the 3PB specimens, with a/W = 0.5(b = B) and 0.2(b >> B), and a CCT specimen with 2a/W = 0.52(b >> B) (see Table 1) was simulated numerically with the ABAQUS 'debond' process (only available for 2-D meshes). A rectangular finite element mesh at the crack tip region is required for incremental crack extension. Crack propagation criteria can be specified in three ways in ABAQUS, namely critical crack opening displacement, critical stress and crack length versus time (which is related to the time period of the analysis). Elements and nodes associated with the two potential crack surfaces are specified in pairs which are initially contacted, but can be separated using one of the prescribed crack propagation criteria, under the debond operation.

The critical crack opening displacement (COD) criterion is used typically for crack propagation in ductile materials, and is used in the present case. For this criterion, the user inputs a relationship between the COD and the crack extension. A fixed distance, measured from the current crack tip, locates the point where the COD is monitored, which is not usually at the crack tip for reasons of precision. The crack propagates progressively (from one node to another) as a function of the prescribed crack extension and the ratio of current (computed) COD to the prescribed COD. In the debond process used in the present case, stresses between the two initially contacted elements reduce to zero as a step function when the separation begins.

No experimental crack extension data was available for the numerical analysis, but a curve relating the load and crack mouth opening displacement (CMOD) was provided. Using simple geometry, the COD values versus crack extension required for the ABAQUS input could be estimated on a trial and error basis. The computation proceeded by dividing the debond process into several trials which allowed the load versus CMOD curve of the numerical result to match the experimental result when satisfactory crack extensions had been selected (Figure 2). Within each load increment there were several

increments of crack extension. This procedure was very time consuming, but provided the required results and a good match between the experimental and numerical load-CMOD curves, see Figure 2.

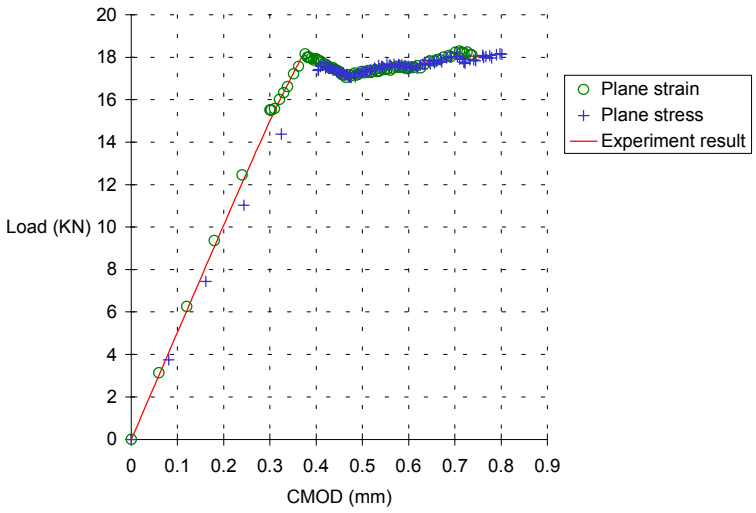

a. a/W = 0.5 (b = B)

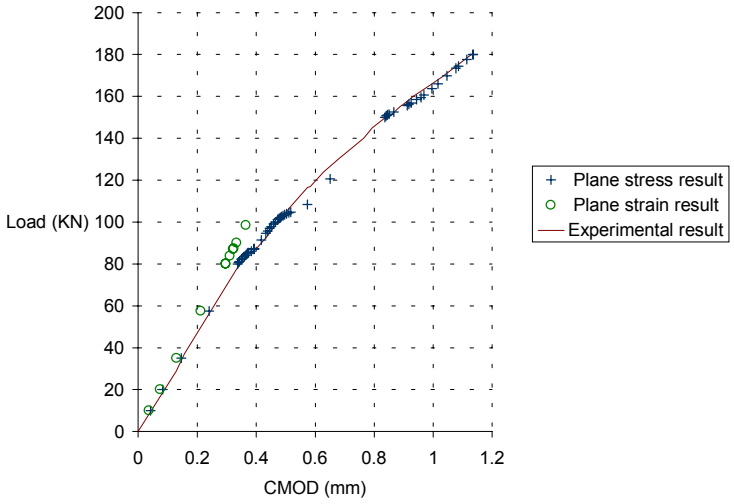

b. a/W = 0.2 (b >> B)

Fig. 2. The comparison of load vs. CMOD plots between numerical and experimental results of 3PB specimens.

Meshes of half of the 3PB specimens and a quarter of the CCT specimen were generated for the 2-D analysis. The three rollers in the 3PB experimental test were modelled as rigid surfaces, which had no deformation when they contacted with the

model of the specimen. The roller positioned above the crack line loaded the model. The use of applied loads was recommended by ABAQUS for accurate evaluation of the work done to the model. The output of each increment of crack extension from ABAQUS was calculated after the application of load. In this case the released energy due to crack extension could not be separated from the energy change under increasing load. Therefore the fracture resistance was studied in terms of a J-integral (J_R) versus crack extension (Δa).

OUT-OF-PLANE CONSTRAINT

The numerical analysis, being 2-D, does not model the actual physical separation of the test piece, but gives a through-thickness average of the plasticity with increasing crack extension. This average can be understood in terms of a mixture of 'slant' and 'flat' plasticity at any particular average crack extension, with the slant component quickly becoming dominant. This mixture must be consistent between different geometries in order to obtain the same R-curve. In addition, there is the choice between either plane strain or plane stress out-of-plane constraint, which effects the extent of in-plane plasticity, and hence the J_R value. Where possible, each specimen was analysed using both constraints, and comparison with experimental data decided the most appropriate constraint. For example, the plane strain J_R-curve of the $a/W = 0.2(b >> B)$ 3PB specimen was not acceptable because the load-CMOD result (see Figure 2b) of the numerical test did not coincide with the experimental record. This was evident before any crack growth, which started at an applied load of 85KN. In addition, the 3-D analysis of this specimen with a stationary crack showed close agreement between 3-D and plane stress load-displacement curves.

Crack tip plastic zones remained small for the extent of the computed crack growth ($\Delta a < 10$mm), whether plane strain or plane stress constraint was used. At crack initiation, plane stress plastic zone ratios, r_y/a, were typically 0.05, and at $\Delta a = 9$mm, $r_y/(a + \Delta a)$ was around 0.26. Small scale yielding applied to this region of crack growth, and differences between plane strain and plane stress computations at crack initiation were small (typically 10%). For a static crack, plane strain analysis gave the best estimate of near crack tip stress and strain fields when compared to a 3-D analysis, but away from the near tip region, plane stress conditions dominated. For a growing crack, the crack tip would quickly grow into a plane stress field, and this was confirmed by examination of experimental data. It was clear that shear lips developed at an early stage, so that the plasticity increased almost from the beginning of crack propagation, resulting in a continuous increase of dJ/da. Hence, it was considered that plane stress analysis gave a better estimate of the crack tip plastic work in the early stages of crack propagation ($\Delta a < 4$mm) rather than plane strain conditions, which existed around the crack tip prior to propagation.

COMPARISON OF J_R CURVES

All the computed R-curves showed the same basic shape, whether computed using plane stress or plane strain conditions, see Figures 3 and 4 for the plane stress curves. The curves were 'concave', showing increasing values of dJ/da with crack extension, which is

the opposite behaviour for more conventional R-curves. The shape corresponded to the change from flat to slant fracture in the region of stable crack extension modelled numerically. The mode of separation on both flat and slant plane remained ductile, and showed the same microstructural characteristics.

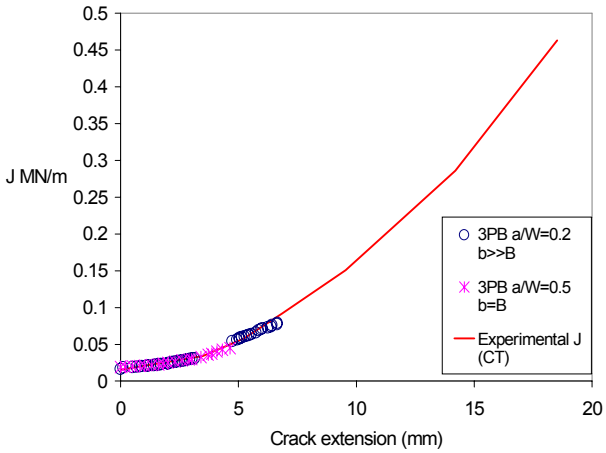

Fig. 3. The J_R-curves from numerical and experimental results.

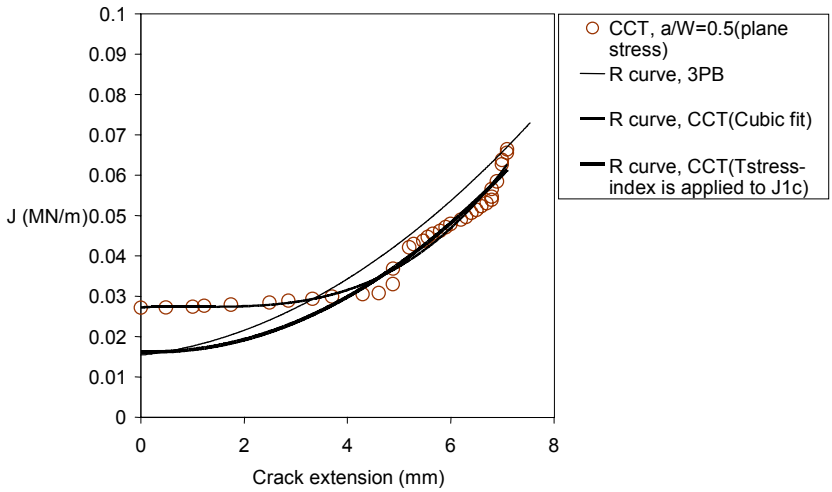

Fig. 4. Comparison of plane stress JR-curve between 3PB and CCT specimens.

Crack growth in both a/W = 0.5(b = B) and the a/W = 0.2(b >> B) specimens was stable [3], but the load behaviour was different after crack initiation (the specimens were tested using displacement control). The load for the a/W = 0.5 specimen stayed constant within ±10% of the maximum load, Figure 2a, whilst the load for the a/W = 0.2(b >> B) 3PB specimen rose with increasing CMOD, Figure 2b. Both specimens yielded similar R-curves.

The form of the R-curve has since been confirmed experimentally by Sumpter[8], Figure 3, after the numerical analysis was completed. He used a compliance unloading technique (which gives a measure of the average crack extension) on an a/W = 0.23(b >> B) CT specimen to obtain an R-curve for the material, using plane stress calibrations. He used formulae from the ASTM standard [9] (which calculates the J-integral for current crack lengths) to obtain J_e and J_p, and hence $J_R = J_e + J_p$. He provided an R-curve for a crack extension up to 18.5mm (the crack tunnelled, and tapered to a point at $\Delta a = 18.5$mm with a V-shaped cross-section) at which point the specimen failed by unstable V-shaped fracture at 90° to the original notch direction. Another fracture test by Sumpter [8] on an a/W = 0.5(b >> B) CT specimen provided a similar J_R-curve for a crack extension of 35mm. The numerical plane stress R-curve from the large ligament 3PB specimen agrees closely with the experimental result from the CT specimen, see Figure 3. Both 3PB and CT specimens are high constraint geometries.

The higher J at initiation for the CCT test result (a low constraint geometry) in Figure 4 is correlated to a negative T-stress, which is rationalised by the J_C-T locus, Figure 1. As the J_R-curve rises with crack extension, the curves from the CCT and 3PB (b >> B) specimens converge, because the effects of in-plane constraint becomes insignificant due to increasing amounts of slant fracture. The curve with the thicker line in Figure 4 is an estimate of how the CCT curve would look when corrected for zero T-stress, hence reducing J to 0.018MN/m at initiation. This estimated curve is close to the high constraint J_R-curve obtained from the 3PB specimen.

APPLICATION OF THE CONSTRAINT CORRECTED R-CURVE

For materials under elastic behaviour, the driving force (G) defines the change of potential energy (U_e) per unit crack growth, (dU_e/da). The crack propagates in a stable fashion when [11]

$$G = R$$

and

$$\frac{dG}{da} \leq \frac{dR}{da}$$

whereas for unstable crack growth;

$$\frac{dG}{da} > \frac{dR}{da}$$

where R is the fracture resistance.

Fracture tests [3] on the AlMgZn alloy showed that shallow cracks in small (b = B) specimens failed at K_{1C}, while in specimens with b >> B, failure was preceded by stable crack growth. Instability prediction for three different 3PB specimens (all tested experimentally), see Table 2, is assessed in this section to demonstrate fracture prediction using the R-curve approach. Assuming the (experimental) plane stress J_R curve and its J_R at initiation are independent of the crack tip condition and specimen geometry (i.e. ignoring the T-stress effects), the invariant J_R curve is reproduced for all crack geometries. Instability of a crack geometry is determined graphically by comparing the calculated driving force curve for the three geometries and the J_R-curve. If the driving force curve lies above the R-curve, then instability will occur at K_{IC}, and vice-versa. If the two curves cross, then instability can follow crack stability, or vice-versa.

Table 2. Details of the 3PB and CT specimen.

3PB specimens a/W	Ligament length, b (mm)	Crack length, a (mm)	Span, S (mm)	Thickness, B (mm)
0.1	25	2.5	110	25
0.5	25	25	200	25
0.2(b>>B)	160	40	800	25

In this report, the driving force, G, is calculated using the solution in BS 7448:Part 1 [11] with an effective crack length to produce a plasticity corrected G_{eff}. Small scale yielding is assumed because the finite element computations of the J_R-curve have only shown this behaviour. The plasticity correction makes a marginal correction to the elastic value.

The G_{eff} curves in Figure 5 are evaluated for constant load with increasing crack length, i.e. increasing a/W ratios. The G_{eff} is calculated for the maximum applied load in the experimental test. An invariant (high constraint) R-curve is produced for each initial crack length.

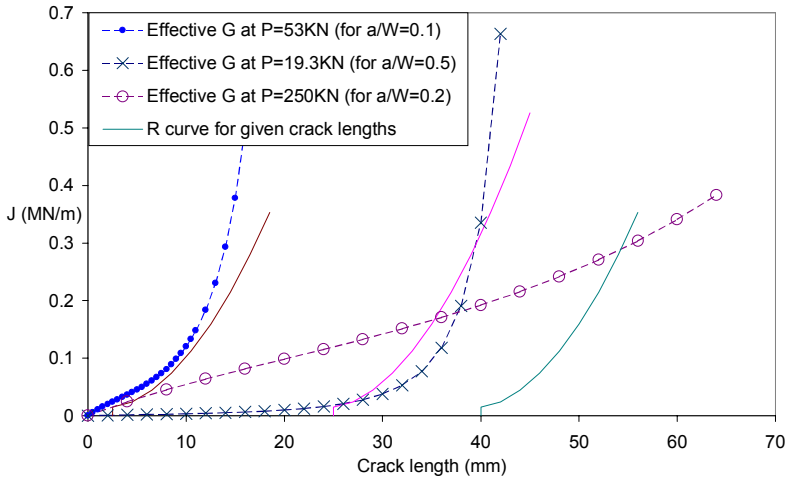

Fig. 5. Instability prediction using R-curve approach for 3PB specimens of a/W = 0.1(b = B), 0.5(b = B) and 0.2(b >> B).

For the specimen with a/W = 0.1(b = B), the G_{eff} curve increases more rapidly than the J_R-curve, indicating that this specimen fails by unstable fracture at the applied load. The G_{eff} at initiation for this specimen was much larger than the J_R value. This high G value is associated with a negative T-stress, which raises the value of J at initiation. In this case, $T/\sigma_{ys} = -0.35$ [10], corresponding to $J_C = 0.03$MN/m using the constraint index [3], see Figure 1, while the computed G_{eff} in Figure 5 is 0.028MN/m.

The G_{eff} at initiation for the specimen with a/W = 0.5(b = B) is slightly larger than the J_R value, but dG/da is just less than dJ_R/da, and hence, initially, the crack extension can be stable. However, G_{eff} increases rapidly with Δa, and soon $dG/da > dJ_R/da$, allowing the G_{eff} curve to cross the J_R-curve. This is potentially an unstable situation in load control,

because small increases in load can increase G_{eff} significantly. Cracks in specimens with square ligaments (b = B) are known to be unstable under load control.

The G_{eff} curve for the a/W = 0.2(b >> B) crosses the J_R-curve (Figure 5), but dG/da is much less than dJ_R/da at this point, and crack growth can only continue by increasing the load. This coincides with the result of experimental test, which was stopped at a final load of 247KN. The crack extension record of this test was not available. This specimen is the closest to the structural situation.

All the above conclusions agree with the experimental observations [3].

SHEAR LIP MODEL

The parabolic nature of the R-curves suggested that a simple shear lip model might explain the R-curve behaviour. Krafft *et al* [12] provided an empirical relationship between the growth of shear lips and fracture resistance, on the basis of three assumptions,

i. the shear lips were at 45° to the crack plane and the region bounded by these two lines was a plastic deformation zone;
ii. this plastic zone was subjected to a constant plastic-work density, dW_p/dV, for all thicknesses of shear lips, at any stage of its formation;
iii. the energy to create new surfaces (dW_e/dA) was supplied for the surface of flat fracture in the central region and for the projected surface of slant shear lips, i.e. the surface that was the product of the thickness and the extended crack length.

If S was the ratio of the total width of shear lips to the thickness, Figure 6, the total plastic deformation zone on the crack flanks was $(BS)^2/2$. An increment of work, dW, for a growing crack was composed of an 'areal' (flat fracture) and volumetric (plastic deformation) components,

$$dW_t = \frac{dW_e}{dA} B da + \frac{dW_p}{dV} \frac{(BS)^2}{2} da \,. \tag{1}$$

where $\frac{dW_t}{da}$ = total energy consumption per unit crack extension,

$\frac{dW_e}{dA}$ = energy consumption per unit crack growth area,

$\frac{dW_p}{dV}$ = energy consumption per unit volume of shear lip,

Krafft *et al*[12] showed that the dW_e/dA and dW_p/dV could be determined from the plot of R versus $BS^2/2$ data from a test. From the results of their tests on 7075-T6 alloy, they found dW_e/dA and dW_p/dV to be 68in.lbs/in^2 and 8300in.lbs/in^3 (i.e. 0.012MNm/m^2 and 57.2MNm/m^3) respectively.

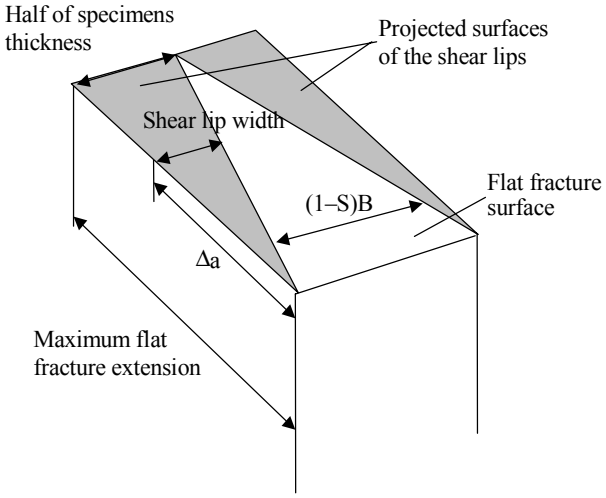

Fig. 6. The projected surface of the shear lips on the plane of flat fracture.

Green and Knott [13] suggested that the fracture of the flat and shear modes were independent, but this made little practical difference to the analysis.

Previous test results [13-15] reported that the width of the shear lips reached a maximum of between 2 to 3mm. It was also proportional to the initial ligament size, i.e. $S/b_0 = 0.2$ and 0.4, in tests on titanium alloy and HY130 steel respectively [14]. Results of fracture testing on the AlMgZn alloy, presented in this paper, show that shear lips can develop across the full 25mm thickness in the large specimens. The fracture mode changed from flat to fully slant in specimens with rectangular ($b >> B$) ligaments, where b is the ligament length.

TRANSITION FROM FLAT TO SLANT FRACTURE

For an initially flat (fatigue) crack, perpendicular to the direction of load in a parallel sided test piece, slant fracture will start at the free surfaces and grow at approximately 45° to the flat fracture, which continues to tunnel in the middle of the specimen. For small test pieces of the AlMgZn alloy, with approximately square ligaments, the shear lips appear to reach some maximum value, as reported for other alloys [13-15]. In 10mm thick CT specimens with square ligaments, Sumpter [8] observed shear lips reaching a maximum width of 2mm, but in the 25mm thick CT specimens of the AlMgZn alloy, the CT specimens with the crack in the LT orientation of the extrusion had maximum shear lips of 5mm per surface.

For large ligament CT specimens, complete transitions from flat to slant fracture were observed in 10 and 25mm thicknesses. After the transition was completed, crack growth continued by slant fracture alone [8]. Complete transitions were also reported by Sumpter [3] in 25mm thick large ligament 3PB and CCT test pieces. The main difference between the transition in the three 25mm thick geometries was the amount of crack extension, Δa_{trans}, required to complete the transition: 18mm for the CT ($a/W = 0.2$), 28mm in the

3PB (a/W = 0.2), and 25mm in the CCT (a/W = 0.5). For the 10mm thick large ligament specimen (a/W = 0.5), complete transition occurred after 6 mm of crack extension.

The reason for the transition from flat to slant fracture is not entirely clear. Shear lips will saturate when the rate of change of the applied energy release rate exceeds the rate of change of fracture resistance [16].

SHEAR LIP ANALYSIS

The J_R curves for all the large ligament specimens used in this analysis are given in Figures 3 and 4. Using the model due to Krafft *et al*, equation (1), the energy per unit crack growth, i.e. BdW_e/dA, is constant for the full range of crack extension, and J can be plotted against $BS^2/2$ to give a linear plot. The data used for the shear lip analysis was taken from the curves fitted to the R-curve values by the least squares method.

For the low constraint CCT specimen, the J_R curve is not parabolic, because of the elevation of the initiation J_R value by the loss of constraint. Figure 4 shows that this curve can be fitted satisfactorily (using least squares) by a cubic polynomial with the following equation:

$$J = 0.1558\Delta a^3 - 0.46\Delta a^2 + 0.4253\Delta a + 27.282 \quad (\text{N/mm}) \tag{2}$$

The first 2–3 millimetres of this curve are almost linear, and it is possible, by suitable manipulation, to split equation (2) into an initial linear section, covering the first 2mm of crack growth, and a parabolic curve covering the remaining crack growth. The computation of the parabolic equation from (2) is very sensitive to the values of the first two coefficients in equation (2). It was found more satisfactory to fit a parabola by least squares in the region $\Delta a = 3$ to 8mm, but including the J_R initiation value obtained from the J-T indexing curve, see Figure 4. This latter parabola was the J_R curve used in the shear lip analysis for the CCT specimen, and was very similar to the J_R curves computed directly from the measured data, see Figure 4.

The first 2-3mm of crack growth is covered by the pop-in observed in the load v. clip gauge displacement curve.

The J_R curves computed by the finite element method (3PB with a/W = 0.2 and 0.5, and the CCT specimen) only covered the first 8-9 mm of crack extension. The experimental curve for the CT specimen, provided by Sumpter [5], covered a crack extension of 18mm, after which the specimen failed in the transverse direction. A detailed photograph was available to the authors for this specimen, and the shear lip width at several crack extensions could be measured with good accuracy. These measurements were used to plot J_R versus $BS^2/2$, Figure 7, which shows a reasonable linear variation, although with some deviation associated with the slight curvature of the shear lip shape (this deviation could also be used to justify the Knott model [13]). For the 3PB and CCT specimens, the photographs could only be used to estimate the transition range, Δa_{trans}, and a linear variation between S and the crack extension was assumed.

The results are given in Table 3, which gives the values of dW_p/dV and dW_e/da, as well as the transition range, Δa_{trans}.

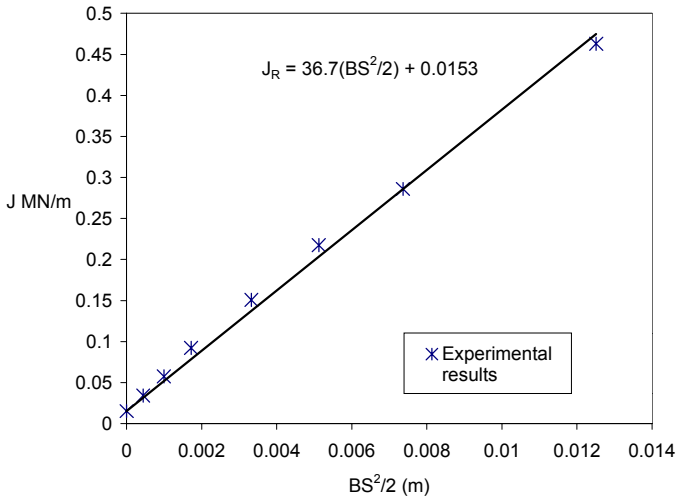

Fig. 7. Plot of J_R versus $BS^2/2$ for CT specimen to determine elastic and plastic work rates from the Krafft *et al* model.

Table 3. Elastic and plastic work rates from shear lip analysis

Specimen	3PB (a/W = 0.2)	CCT (a/W = 0.5)	CT (a/W = 0.2)
Krafft dW_P/dV (MNm/m^3)	64.0	53.7	36.7
dW_e/dA (MNm/m^2)	0.017	0.016	0.015
Δa_{trans} (mm)	28	25	18
$(dW_P/dV)/\Delta a_{trans}$ (MN/m^3)	2285	2148	2039
Cone dW_p/dV (MNm/m^3)	18.2	17.1	16.2

The range of values for dW_P/dV scale with the transition distance, Δa_{trans}, which is not unexpected. A constant dW_P/dV for all geometries, plus a single, independent, R-curve implies a constant Δa_{trans}. The Krafft model only considers the variation of the shear lips through the thickness, and does not consider the effects of in-plane changes in plastic zone size. The finite element analysis showed the plane stress plastic zones at initiation were approximately circular, and centred on the crack tip. If we assume that the plastic deformation at any crack extension is contained within two cones, of height BS/2 and radius $S\Delta a_{trans}$ (which keeps one edge of the cones coincident with their starting point) then the volume of the cone is given by $(\pi/3)(BS/2)(S\Delta a_{trans})^2$. Differentiating, we have

$$dV = \pi\left(\frac{BS^2}{2}\right)\Delta a_{trans}{}^2 dS = \pi\left(\frac{BS^2}{2}\right)\Delta a_{trans}\, da \tag{3}$$

as $dS = da/\Delta a_{trans}$. Substituting into equation (1), the coefficient for dW_p/dV now becomes $(\pi S^2 \Delta a_{trans}/2)$, instead of $(BS^2/2)$. Modifying the original Krafft analysis for the cone assumption, we get the values for dW_p/dV shown in line 5 of table 3, by multiplying line 4 by B/π.

This analysis gives reasonable constant estimates for dW_p/dV, but loses the 45^o boundary for the shear lips. These boundaries now vary with geometry, as they are dependent on Δa_{trans}, producing much steeper slant boundaries. A more detailed analysis, assuming an elliptical plastic zone on the surface, did not give consistent results.

CONCLUSIONS

The increase of fracture resistance (compared with the plane strain K_{IC}) during large-scale fracture testing was due to a combination of low constraint and stable crack extension. The elevated fracture toughness for low constraint geometry could be indexed by negative T-stresses. Fracture assessment, using a T-stress indexed fracture toughness alone, underestimates the critical crack length in structural components.

Numerical analysis of stable crack extension produced a concave J_R-curve, and this was confirmed later by experimental evaluations. After corrections for the T-stress, a reasonably geometry independent R-curve was obtained. The concave shape was associated with the developments of shear lips. Fracture assessment using the R-curve approach showed that the extension of a crack in large ligament ($b >> B$) specimens of the alloy are stable because $dG/da < dJ_R/da$, caused by dJ_R/da increasing with Δa. For shallow cracks in small ($b = B$) specimens, initial instability leads to final fracture. The prediction of instability using the R-curve approach in small ($b = B$) and large ($b >> B$) specimens agreed with experimental observations.

The difference of J_R between 3PB (a high constraint geometry) and CCT (a low constraint geometry) specimens at initiation is the result of in-plane constraint effects, which can be represented by the T-stress in this study. The J_R-curve for high and low constraint geometries converged after 3mm or so of crack extension. The R-curve approach must be corrected by T-stresses when it is applied to low constraint geometries. The J_C value is therefore correlated to Δa and T-stresses.

A shear lip model was used to explain the 'concave' R-curve, based on the work of Krafft *et al* [1]. The model gave a good fit to the R-curve, but the plastic work rate, dWp/dV, was not constant for the different test piece geometry. It was found that this work rate could be scaled by the transition crack extension, Δa_{trans}, i.e. the crack extension in which the mode of fracture changed from fully flat to fully slant. A 'cone' model gave consistent values for dWp/dV, but sacrificed the 45^o shear lip assumption of Krafft *et al*. More detailed analysis is required.

Acknowledgements. *The author thanks Dr. J. D. G. Sumpter of the Defence and Evaluation Research Agency, UK, for providing all the experimental data used in this paper, and the Agency for permission to publish the data*.

REFERENCES

1. Webber, D., (1985) Fatigue Design and Testing of an AlZnMg Alloy Bridge Girder, Royal Armament Research and Development Establishment, Christchurch, Dorset, presented at the Third International Conference on Aluminium Weldments, Munchen.
2. Henry, B.S., and Luxmoore, A.R., (1996) Two-Parameter Fracture Assessment of Through-Thickness Cracks in an Aluminium Bridge Structure, Eleventh European Conference on Fracture, ECF-11, Futuroscope, France, pp.2145-2150.

3. Sumpter, J.D.G., (1996) Observations on Tearing Instability in an Aluminium Alloy, Mechanisms and Mechanics of Damage and Failure, ECF-11, Vol. 2, pp.855-860.
4. Henry, B.S., Luxmoore, A.R. and Sumpter, J.D.G., (1996) Elastic-Plastic Fracture Mechanics Assessment of Low Constraint Aluminium Test Specimens, International Journal of Fracture Vol. 81, , pp.217-234.
5. Rice, J.R., (1974) Limitation to Small Scale Yielding Approximation for Crack Tip Plasticity, Journal of the Mechanics and Physics of Solids, Vol. 22, pp. 17-26.
6. O'Dowd, N.P. and Shih, C.F., (1992) Two-Parameter Fracture Mechanics: Theory and Applications, ASTM 24th National Symposium on Fracture Mechanics, Tennessee.
7. Henry, B.S., Constraint Based Fracture Assessment of Through-Thickness Cracks in a Bridge Girder Structure, Ph.D. Thesis C/PH/194/96, Department of Civil Engineering, University of Wales Swansea, March 1996.
8. Sumpter, J.D.G., Fracture and Fatigue Testing of a 7019 Aluminium Bridging Extrusion, Restricted commercial report, Defence and Evaluation Research Agency, UK, November 2000.
9. ASTM E 1820-99a, (2000) Standard Test Method for Measurement of Fracture Toughness, American Society for Testing and Materials,
10. Anderson, T.L., (1995) Fracture Mechanics-Fundamentals and Applications, Department of Mechanical Engineering, Texas A&M University, College Station, Texas, CRC Press, Inc., Second Edition,
11. BS 7448 Part 1, (1991) Fracture Mechanics Toughness Tests, British Standard Institution.
12. Krafft, J.M., Sullivan, A.M. and Boyle, R.W., (1962) Effect of Dimensions on Fast Fracture Instability of Notched Sheets, Proceedings of the Crack Propagation Symposium Cranfield, The College of Aeronautics, Vol. 1, pp. 8-28.
13. Green, G. and Knott, J.F., (1975) On Effects of Thickness on Ductile Crack Growth in Mild Steel, Journal of the Mechanics and Physics of Solids, Vol. 23, pp. 167-183.
14. Turner, C.E. and Braga, L., (1993) Energy Dissipation rate and Crack Opening Angle Analyses of Fully Plastic Ductile Tearing, Constraint Effects in Fracture, ASTM STP 1171, American Society For Testing and Materials, Philadelphia, pp. 158-175.
15. Gibson, G.P., Druce, S.G. and Turner, C.E., (1988) Effect of Specimen Size and Geometry on Ductile Crack Growth Resistance in a C-Mn Steel, International Journal of Fracture Vol. 37, pp. 83-100.
16. Cheung, S. and Luxmoore, A.R., A Finite Element Analysis of Stable Crack Growth in an Aluminium Alloy, to be published in Engineering Fracture Mechanics.

PROCENA NAPREDOVANJA STABILNE PRSLINE U ALUMINIJUMSKOJ LEGURI PO R-KRIVULJI

A. R. Luxmoore

AlMgZn legura pokazala se krtom kada je testirana korišćenjem standardnih lomnih uzoraka, ali su veći uzorci sa istom konturnom geometrijom dali stabilan lom, tj. kontrolisano prostiranje prsline ili pod rastućim opterećenjem, ili pod rastućim pomeranjem. Analiza po R-krivulji dala je R-krivulju za leguru koja je prilično neobičnog oblika, ali jedinstvena, kod koje se otpornost prsline parabolično povećava sa prostiranjem prsline. Pored toga, zapodinjanje prsline bilo je indeksirano ograničenjem testnog uzorka. Uprkos ovim komplikacijama, analiza po R-krivulji dala je zadovoljavajuće objašnjenje za različito ponašanje pri lomu malih i velikih testnih uzoraka. Parabolična priroda R-krivulje, koja je dobijena iz više različitih geometrija, sugeriše da bi jednostavna analiza po smicajnoj ivici, slična Kraftovoj, Bojlovoj i Salivenovoj, trebalo da objasni ponašanje testnih delova, ali uprkos odredjenim izmenama prvobitne teorije smicajne ivice, rezultati nisu uverljivi.